

Systematic Regge theory analysis of omega photoproduction

A. Sibirtsev¹, K. Tsushima^{1,2,3} and S. Krewald^{1,2}

¹*Institut für Kernphysik,*

Forschungszentrum Jülich, D-52425 Jülich

²*Special Research Center for the Subatomic Structure of Matter (CSSM) and Department of Physics and Mathematical Physics, University of Adelaide, SA 5005, Australia*

³*Department of Physics and Astronomy, University of Georgia, Athens, GA 30602 USA*

Systematic analysis of available data for ω -meson photoproduction is given in frame of Regge theory. At photon energies above 20 GeV the $\gamma+p \rightarrow \omega+p$ reaction is entirely dominated by Pomeron exchange. However, it was found that Pomeron exchange model can not reproduce the $\gamma+p \rightarrow \rho+p$ and $\gamma+p \rightarrow \omega+p$ data at high energies simultaneously with the same set of parameters. The comparison between ρ and ω data indicates a large room for meson exchange contribution to ω -meson photoproduction at low energies. It was found that at low energies the dominant contribution comes from π and f_2 -meson exchanges. There is smooth transition between the meson exchange model at low energies and Regge theory at high energies.

PACS numbers: 13.60.Le; 13.88.+e; 14.20.Gk; 25.20.Lj

I. INTRODUCTION

The vector meson photoproduction at high energies is traditionally discussed in terms of Regge theory. The most recent systematic theoretical analysis [1, 2, 3] confirmed that at high energies the photoproduction of ρ - and ϕ -meson can be well described by soft Pomeron and meson Regge trajectories.

ZEUS data [4] at high energies on ρ -meson photoproduction at $|t|$ above $\simeq 0.4 \text{ GeV}^2$ need additional contribution from hard Pomeron exchange [5]. Furthermore, very recent CLAS data on ρ - [6] and ϕ -meson [7] photoproduction at $E_\gamma \simeq 3. \div 4 \text{ GeV}$ can be well explained by Regge theory at low momentum transfer $|t| \leq 1 \text{ GeV}^2$.

The Regge theory calculations [2, 8] for ρ -meson photoproduction at low $|t|$ indicates that at low energies the dominant contribution comes from f_2 -meson exchange, while at high energies it is due to Pomeron exchange. The ϕ - and J/Ψ -meson photoproduction at small momentum transfers are dominated by Pomeron exchange because of the $s\bar{s}$ and $c\bar{c}$ structure of these mesons [9], respectively.

At backward angles, where $|u|$ is small, the ρ -meson photoproduction is dominated by exchange of nucleon and Δ Regge trajectories in the u channel. The backward ϕ -meson photoproduction is due to the u -channel nucleon exchange.

Moreover, the recent data [6, 7] on ρ and ϕ -meson photoproduction at both large $|t| > 1 \text{ GeV}^2$ and large $|u|$ had been interpreted as due to the hard scattering between the photon and the quarks in the nucleon.

While ρ and ϕ -meson photoproduction were systematically studied within the Regge theory, the ω -meson photoproduction data have been analyzed only selectively. As is shown in Refs. [3, 8] the calculation with the inclusion of π , f_2 and Pomeron trajectory exchanges un-

derestimate experimental data on total $\gamma+p \rightarrow \omega+p$ cross section at $E_\gamma \geq 50 \text{ GeV}$. It is important that at these high energies the photoproduction is dominated by Pomeron exchange and it is strongly believed [1, 2] that the Regge theory is able to describe the total cross section for the ω as well as for the ρ - and ϕ -meson photoproduction.

To get an overview about the Regge theory for ω -meson photoproduction we perform a systematic analysis of available data.

II. THE POMERON EXCHANGE

The mechanism responsible for elastic vector meson photoproduction at high energies was originally identified as Pomeron exchange [1, 2] within the phenomenological Regge model [10]. Recently, there was an apparent development in the description of Pomeron exchange in terms of the quark and gluon degrees of freedom of QCD [11] as an underlying theory of strong interactions.

The concept of the model is based [12] on that a photon fluctuates into the vector meson, and interacts with the quark, among those confined in the vector meson and the nucleon through the Pomeron exchange. The structure of the quark-nucleon Pomeron exchange interaction and the most general expression for the amplitude \mathcal{T}_P for the vector meson production by virtual photon were given by Donnachie and Landshoff [12] as

$$\mathcal{T}_{P_1} = 3i F_1(t) \frac{8\sqrt{6} m_q e_q f_V \beta_0^2}{Q^2 + 4m_q^2 - t} (\varepsilon \cdot \varepsilon_V) \left(\frac{s}{s_0} \right)^{\alpha_{P_1}(t)-1} \times \exp\left[\frac{-i\pi(\alpha_{P_1}(t)-1)}{2} \right] \frac{\mu_0^2}{2\mu_0^2 + Q^2 + 4m_q^2 - t}, \quad (1)$$

where the proton isoscalar electromagnetic (EM) form

factor $F_1(t)$ is given by

$$F_1(t) = \frac{4m_p^2 - 2.8t}{4m_p^2 - t} \frac{1}{(1 - t/t_0)^2}, \quad (2)$$

where m_p is the proton mass and $t_0=0.7 \text{ GeV}^2$. Furthermore, s is invariant collision energy squared, and Q^2 denotes the squared mass of the virtual photon and t is the four momentum transfer squared between the photon and vector meson. In Eq.(1) e_q and m_q are the quark effective charge and mass, respectively, while ϵ and ϵ_V are the polarization vectors of the virtual photon and vector meson, respectively. Finally f_V is the vector meson radiative decay coupling constant given by $V \rightarrow e^+e^-$ decay width.

Free phenomenological parameters are β_0 and μ_0 . The parameter β_0 determines the strength of the effective coupling of the Pomeron to quark, while the parameter μ_0 accounts that the coupling is not point-like and it is dressed with the form factor given by the last term of Eq.(1). The experimental values of β_0 and μ_0 were evaluated from the high energy elastic and inelastic scattering at small $|t|$,

and are given as [13, 14, 15]

$$\beta_0 = 2.0 \text{ GeV}^{-1}, \quad \mu_0 = 1.1 \text{ GeV}. \quad (3)$$

Furthermore, the Pomeron trajectory $\alpha_{P_1}(t)$ is given by [16]

$$\alpha_{P_1}(t) = 1 + \epsilon + \alpha'_{P_1} t, \quad (4)$$

with $\epsilon=0.08$ and $\alpha'_{P_1}=0.25 \text{ GeV}^{-2}$. The constant s_0 is not well determined theoretically, however within the dual model prescription [17] it can be taken as $s_0=1/\alpha'_{P_1}$.

Finally, the differential $\gamma+p \rightarrow V+p$ cross section $d\sigma/dt$ due to Pomeron exchange is given for a real photon,

$$\frac{d\sigma}{dt} = \frac{81 m_V^3 \beta_0^4 \mu_0^4 \Gamma_{e^+e^-}}{\pi \alpha} \left(\frac{s}{s_0} \right)^{2\alpha_{P_1}(t)-2} \times \frac{F_1^2(t)}{(m_V^2 - t)^2 (2\mu_0^2 + m_V^2 - t)^2}, \quad (5)$$

where $m_V=2m_q$ is the vector meson mass, $\Gamma_{e^+e^-}$ is the partial $V \rightarrow e^+e^-$ decay width and α is electromagnetic coupling constant.

The dashed lines in Fig.1 show the contribution from Pomeron exchange to the differential $\gamma+p \rightarrow \omega+p$ cross section as a function of four momentum transfer squared t . The circles in Fig.1 indicate the FNAL data [18] collected at photon energies $50 \leq E_\gamma \leq 130 \text{ GeV}$, while the squares show the DESY ZEUS data [19] at invariant collision energy $70 \leq \sqrt{s} \leq 90 \text{ GeV}$. Obviously the calculations by Eq.(5) with $\beta_0=2.0 \text{ GeV}^{-1}$ underestimate the data by a factor 1.9.

Most recently the parameters of the Pomeron exchange were readjusted [20] to $\gamma+p \rightarrow \omega+p$ data, which can be well reproduced with the coupling constant, $\beta_0=2.35 \text{ GeV}^{-1}$. We also note that the same value of the coupling constant was deduced [11] from an analysis of $\pi+p$ elastic scattering data at high energies.

The Pomeron parameters were also fixed [2, 21] with the $\gamma+p \rightarrow \rho^0+p$ data. It was assumed that at high energies the contribution from Pomeron exchange to the total $\rho+p$ cross section is the same as to the averaged total π^++p and π^-+p cross sections. Then the vector dominance model through the $\gamma\rho$ conversion was applied. Finally, the phenomenological Pomeron exchange amplitude was given as

$$\mathcal{T}_{P_1} = i A_{P_1} F_1(t) G(t) \left(\frac{s}{s_0} \right)^{\alpha_{P_1}(t)-1} \exp\left[\frac{-i\pi(\alpha_{P_1}(t)-1)}{2} \right], \quad (6)$$

with the proton EM form factor of Eq.(2). The amplitude is normalized such that $d\sigma/dt=|\mathcal{T}|^2$ in μbGeV^{-2} . The Pomeron trajectory was defined by Eq.(4), while the $\gamma\rho$ vertex function $G(t)$ was fitted [2] to the $\gamma+p \rightarrow \rho^0+p$ data as

$$G(t) = \frac{1}{1 - t/0.71}. \quad (7)$$

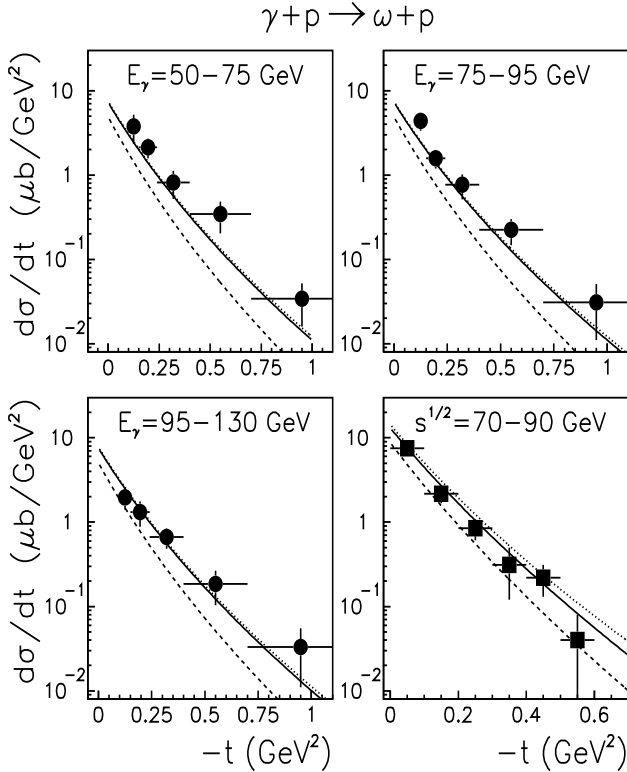


FIG. 1: Differential cross section for $\gamma+p \rightarrow \omega+p$ as a function of four momentum transfer squared t , at different photon energies E_γ , or invariant collision energy \sqrt{s} . The circles show experimental results from FNAL [18], while the squares are the data from DESY ZEUS [19]. The lines show the Regge model calculations with Pomeron exchange only: the dashed- by Eq.(5) with fixed parameter $\beta_0=2.0 \text{ GeV}^{-1}$ [13, 14, 15], the solid- by Eq.(6) with soft Pomeron exchange parameters adjusted by the $\gamma+p \rightarrow \omega+p$ data and the dotted- with both soft and hard Pomeron exchanges.

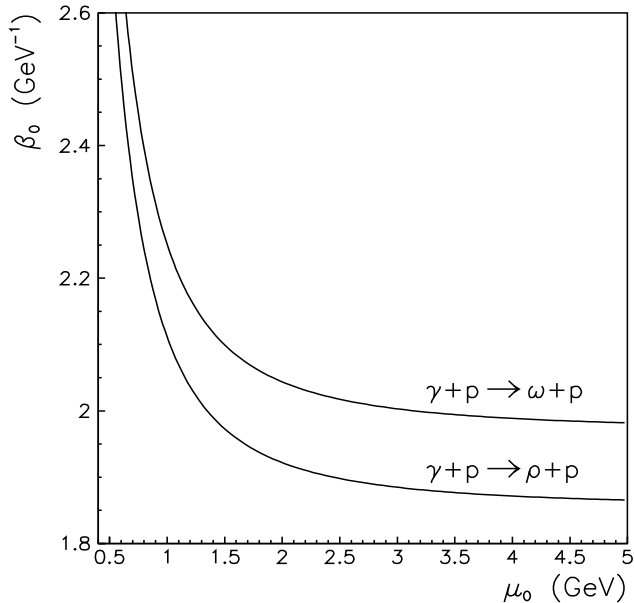


FIG. 2: The solution for μ_0 and β_0 parameters evaluated at $t=0$ by Eq.(8) from phenomenological analysis of $\gamma+p\rightarrow\rho+p$ and $\gamma+p\rightarrow\omega+p$ data.

The normalization constant of Eq.(6) was fitted [2] to the data, and extracted value is $A_{P_1}=0.06$ fm/GeV for the ρ -meson photoproduction.

It is clear that the t -dependence of Eq.(6) differs from that given by Eq.(1). However, at $t=0$ the relation between the normalization constant A_{P_1} and the parameters β_0 and μ_0 of Eq.(6) can be written as

$$\beta_0^4 = \frac{\pi \alpha m_V}{81 \mu_0^4 \Gamma_{e^+e^-}} (2\mu_0^2 + m_V^2)^2 A_{P_1}^2. \quad (8)$$

Fig. 2 shows the solution for μ_0 and β_0 parameters evaluated by Eq.(8) from $A_{P_1}=0.06$ fm/GeV. The parameters given by Eq.(3) are in reasonable agreement with phenomenological analysis [2] of ρ -meson photoproduction.

To reproduce the $\gamma+p\rightarrow\omega+p$ data we adjust the normalization constant in Eq.(6) as $A_{P_1}=0.02$ fm/GeV. The solid lines in Fig. 1 show the calculations using the phenomenological Pomeron exchange amplitude of Eq.(6). The calculations reproduce both the absolute value and t -dependence of the differential cross section, $\gamma+p\rightarrow\omega+p$, at high photon energies.

Fig. 2 also shows the solution for μ_0 and β_0 parameters evaluated by Eq.(8) from $\gamma+p\rightarrow\omega+p$ data. It is clear that Pomeron exchange model can not reproduce the $\gamma+p\rightarrow\rho+p$ and $\gamma+p\rightarrow\omega+p$ data simultaneously with the same set of parameters, μ_0 and β_0 . This result is in agreement with our finding reported in Ref. [20].

Direct experimental illustration [20] of this discrepancy is given by the ratio of the total $\gamma+p\rightarrow\omega+p$ to $\gamma+p\rightarrow\rho^0+p$ cross sections, which is shown in Fig. 3. At photon energies $E_\gamma \geq 6$ GeV it is consistent with SU(3)

predictions and equals to 1/9. Obviously, this ratio is consistent with phenomenological fit given by Eq.(6).

The ratio of the $\gamma+p\rightarrow\omega+p$ to $\gamma+p\rightarrow\rho^0+p$ cross sections from Pomeron exchange model of Eq.(1) equals to the ratio of the $\omega\rightarrow e^+e^-$ and $\rho\rightarrow e^+e^-$ decay widths. The experimental results on $\rho\rightarrow e^+e^-$ and $\omega\rightarrow e^+e^-$ decay widths indicate [22] that the $\gamma\omega$ coupling is 3.4 ± 0.2 times smaller than that for the $\gamma\rho$. Therefore the ratio of the $\gamma+p\rightarrow\omega+p$ to $\gamma+p\rightarrow\rho^0+p$ cross sections is underestimated by $\simeq 28\%$ as compared with the ratio given by the experimental $\rho\rightarrow e^+e^-$ and $\omega\rightarrow e^+e^-$ decay widths, which is shown by the dashed line in Fig. 3.

The DESY ZEUS data on ρ -meson photoproduction at invariant collision energy $\sqrt{s}=71.7$ GeV at four momentum transfer squared $0.4 \leq |t| \leq 1.6$ GeV² require [2] some additional contribution, which may come from the hard Pomeron exchange. The hard Pomeron amplitude is given by

$$\mathcal{T}_{P_0} = i A_{P_0} F_1(t) \left(\frac{s}{s_0} \right)^{\alpha_{P_0}(t)-1} \exp\left[\frac{-i\pi(\alpha_{P_0}(t)-1)}{2} \right], \quad (9)$$

with the proton EM form factor given by Eq.(2).

The hard Pomeron trajectory is fixed by ρ -meson photoproduction data as

$$\alpha_{P_0} = 1.44 + \alpha'_{P_0} t, \quad (10)$$

where $\alpha'_{P_0}=0.1$ GeV⁻². Furthermore, $s_0=1/\alpha'_{P_0}$ and $A_{P_0}=3.6\cdot 10^{-4}$ fm/GeV for ρ -meson photoproduction [2].

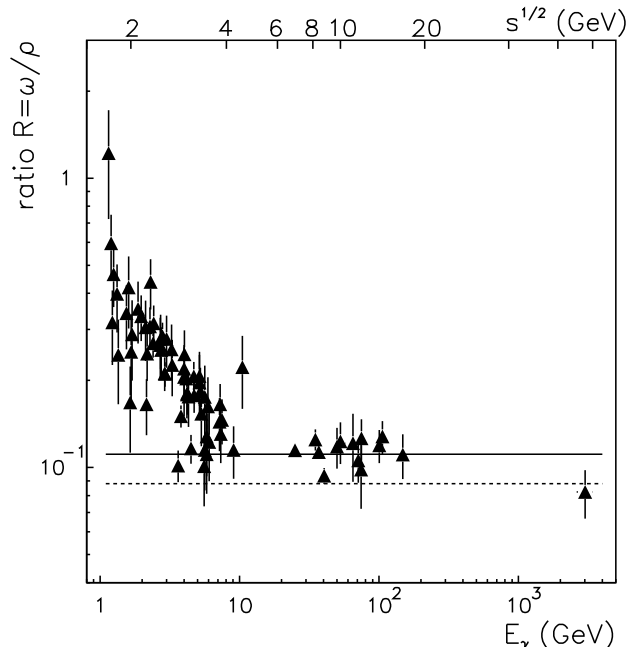


FIG. 3: The ratio of total cross sections, $\gamma+p\rightarrow\omega+p$ to $\gamma+p\rightarrow\rho^0+p$, as a function of photon energy E_γ (lower axis), or invariant collision energy \sqrt{s} (upper axis). The dashed line shows the ratio of $\gamma\omega$ to $\gamma\rho$ coupling constants determined by relevant radiative e^+e^- decay widths. The solid line indicates the ratio expected from SU(3) symmetry.

Following the results for soft Pomeron exchange we readjust $A_{P_0}=1.2\cdot 10^{-4}$ fm/GeV for ω -meson photoproduction.

The $\gamma+p\rightarrow\omega+p$ differential cross section due to the soft P_1 and hard P_0 Pomeron exchanges is finally given as

$$\frac{d\sigma}{dt} = |\mathcal{T}_{P_0} + \mathcal{T}_{P_1}|^2, \quad (11)$$

and is shown in Fig. 1 by the dotted lines. The inclusion of P_0 exchange does not affect the calculations at low $|t|$, but results in non negligible contribution at $70\leq\sqrt{s}\leq 90$ GeV and $0.4\leq|t|$. The absence of the high energy ω -meson photoproduction data at large $|t|$ indeed does not allow presently to clarify the role of hard Pomeron exchange for the $\gamma+p\rightarrow\omega+p$ reaction.

With decreasing the photon energy the contribution from Pomeron exchange to ω -meson photoproduction decreases. This is illustrated by Fig. 4 where the experimental results [23, 24, 25] on differential $\gamma+p\rightarrow\omega+p$ cross section are shown for the photon energies E_γ from 4.7 to

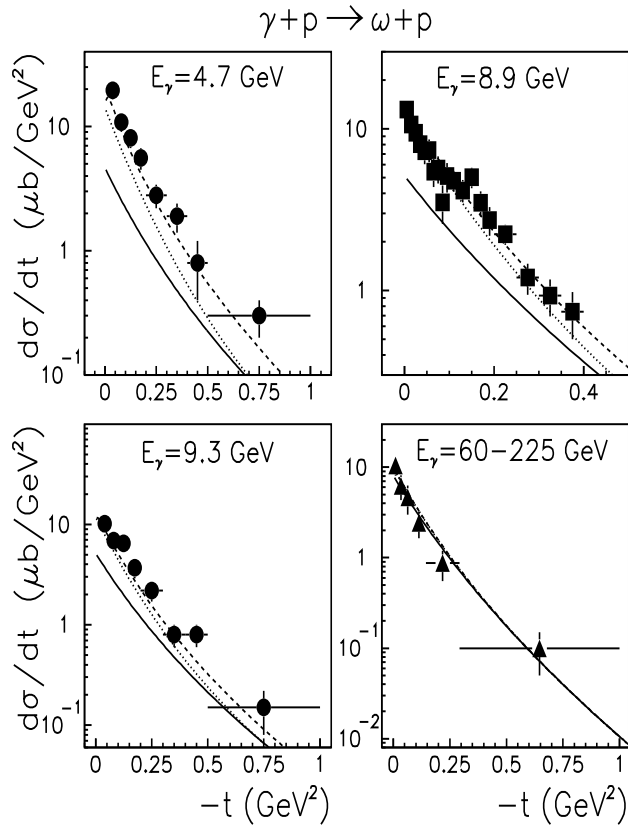


FIG. 4: Differential cross section, $\gamma+p\rightarrow\omega+p$ as a function of four momentum transfer squared t at different photon energies E_γ . Circles show experimental results from SLAC [23], the squares are the CORNELL data [24], while triangles show the FNAL data [25]. The solid lines indicate the calculations with soft and hard Pomeron exchanges, with parameters fitted to the ω -meson photoproduction data. The dotted line shows the results with additional inclusion of f_2 -meson exchange, while the dashed lines are the full model results with π , f_2 and Pomeron exchanges.

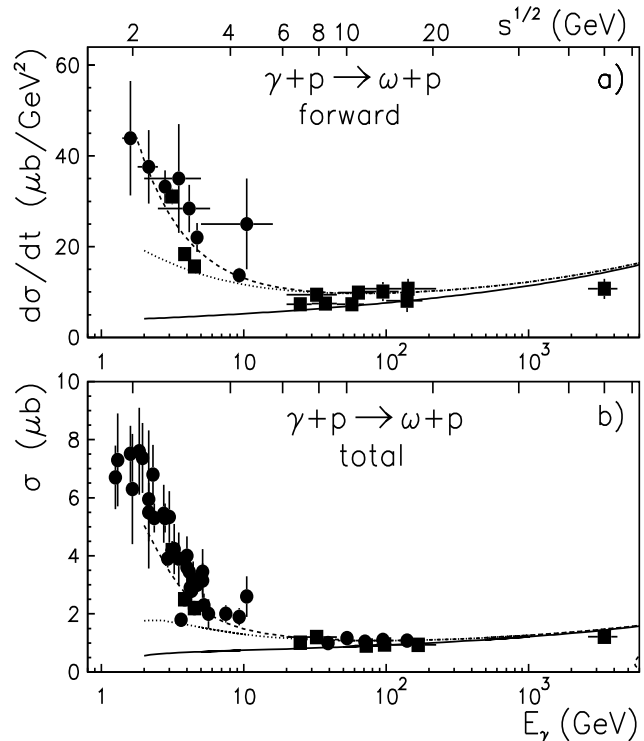


FIG. 5: Forward (extrapolated at $t=0$) (a) and total (b) $\gamma+p\rightarrow\omega+p$ cross sections as a function of photon energy E_γ (lower axis), or invariant collision energy \sqrt{s} (upper axis). The solid lines indicate the calculations with soft and hard Pomeron exchanges. The dotted lines show the results with additional inclusion of f_2 -meson exchange, while the dashed lines are the full model results with π , f_2 and Pomeron exchanges.

225 GeV, together with soft and hard Pomeron exchange calculations, which are indicated by the solid lines.

The analysis [2] of ρ -meson photoproduction shows that at low energies significant contribution comes from f_2 -meson exchange. The contribution from f_2 -meson exchange to the $\gamma+p\rightarrow\omega+p$ reaction will be analyzed in next section.

To summarize our analysis of Pomeron contribution to the ω -meson photoproduction is shown in Fig. 5, for the $\gamma+p\rightarrow\omega+p$ data on total and differential $d\sigma/dt$ cross section extrapolated at $t=0$, together with the Pomeron exchange calculations by Eq.(11) (the solid lines).

The upper horizontal axis of Fig. 5 shows the $\gamma+p$ invariant collision energy, while the lower horizontal axis indicates the photon energy E_γ . It is clear that the Pomeron exchange alone well describes the $\gamma+p\rightarrow\omega+p$ reaction at E_γ above 20 GeV at small $|t|$ and dominates the total ω -meson photoproduction cross section. However, the Pomeron exchange parameters for ω -meson photoproduction differ from that used [2, 3] for $\gamma+p\rightarrow\rho+p$ reaction.

III. THE REGGEONS EXCHANGES

In order to reproduce the ρ -meson photoproduction data at invariant collision energies $\sqrt{s} < 10$ GeV it is necessary to consider the contributions from the next to leading Pomeron ρ , ω and f_2 singularities with an intercept close to $\alpha(t=0) \simeq 0.5$.

However the ρ and ω trajectories can not be exchanged and it was proposed in Refs. [2, 3] that the introduction of the f_2 exchange may be enough to describe the $\gamma+p \rightarrow \omega+p$ data at low energies. The f_2 exchange amplitude is given by [2, 3]

$$\mathcal{T}_f = iA_f F_1(t) G(t) \left(\frac{s}{s_0} \right)^{\alpha_f(t)-1} \exp\left[\frac{-i\pi(\alpha_f(t)-1)}{2} \right], \quad (12)$$

with Regge trajectory

$$\alpha_f(t) = 0.55 + \alpha'_f t, \quad (13)$$

where $\alpha'_f = 0.93$ GeV $^{-2}$, $F_1(t)$ is proton isoscalar form factor given by Eq.(2), while $G(t)$ is $\gamma\rho$ form factor from Eq.(7). Furthermore, $s_0 = 1/\alpha'_f$ and parameter $A_f = 0.159$ fm/GeV was fitted to the ρ -meson photoproduction data. It is important that the sum of the f_2 and soft and hard Pomeron exchanges amplitude describe well the ρ -meson photoproduction data on differential and total reaction cross sections.

The calculations with f_2 and Pomeron exchanges amplitude for the differential $\gamma+p \rightarrow \omega+p$ cross section at photon energies from 4.7 to 9.3 GeV are shown in Fig. 4 by the dotted lines. We scaled the parameter A_f by the factor of 3 as compared to the ρ -meson photoproduction, and performed the calculations using the value $A_f = 0.053$ fm/GeV for ω -meson photoproduction.

The inclusion of f_2 -meson trajectory substantially improves agreement for the differential $\gamma+p \rightarrow \omega+p$ cross section at photon energies $E_\gamma = 8.9$ and 9.3 GeV. However, it is clear that at $E_\gamma = 4.7$ GeV an additional contribution is necessary in order to reproduce the data. The dotted lines in Fig. 5 show the contribution from f_2 and soft and hard Pomeron exchanges to the forward and total ω -photoproduction cross sections.

In case of ω -meson photoproduction this contribution comes essentially from π -meson exchange. The ρ -meson photoproduction data do not indicate much free room for the π -meson exchange since the $\gamma\rho\pi$ coupling constant given by the $\rho \rightarrow \gamma\pi$ decay width $\simeq 0.1$ MeV is substantially smaller than that for the $\gamma\omega\pi$ given by $\omega \rightarrow \gamma\pi$ decay width of $\simeq 0.7$ MeV.

This fact is as well illustrated by Fig. 3, which shows the ratio of total $\gamma+p \rightarrow \omega+p$ to $\gamma+p \rightarrow \rho^0+p$ cross sections. Substantial enhancement of the ratio at photon energies $E_\gamma \leq 5$ GeV might be due to π -meson exchange contribution to ω -meson photoproduction.

The π -meson exchange amplitude can be parameterized as [27]

$$\mathcal{T}_\pi = \frac{iA_\pi m_V \sqrt{-t}}{t - m_\pi^2} \tilde{G}(t) \left(\frac{s}{s_0} \right)^{\alpha_\pi(t)-1} \exp\left[\frac{-i\pi(\alpha_\pi(t)-1)}{2} \right], \quad (14)$$

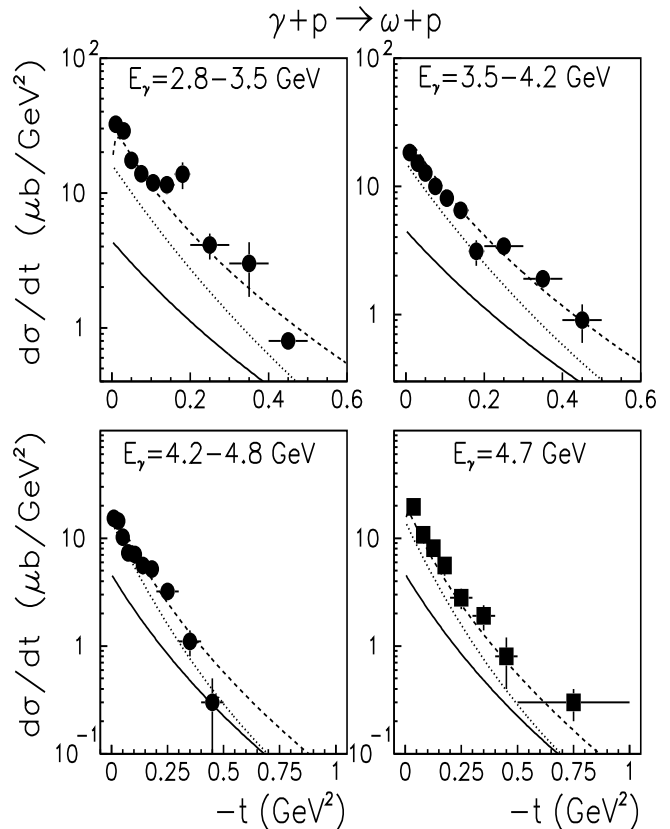


FIG. 6: Differential $\gamma+p \rightarrow \omega+p$ cross section as a function of four momentum transfer squared t at different photon energies E_γ . Squares show the SLAC data [23], while the circles are DARESBUURY experimental data [26]. The solid lines indicate the calculations with Pomeron exchange, the dotted lines show the results with an additional inclusion of f_2 -meson exchange, while the dashed lines are the full model results with π , f_2 and Pomeron exchanges.

with π -meson trajectory given by

$$\alpha_\pi(t) = \alpha'_\pi(t - m_\pi^2), \quad (15)$$

where $\alpha'_\pi = 0.7$ GeV $^{-2}$, m_π is π -meson mass, $s_0 = 1/\alpha'_\pi$.

In the calculation, the parameter $A_\pi = 0.1$ fm/GeV was adjusted in order to reproduce the differential $\gamma+p \rightarrow \omega+p$ cross section at photon energy $E_\gamma = 4.7$ GeV.

Furthermore, $\tilde{G}(t)$ denotes the form factor in the πNN vertex fitted to the data and given by,

$$\tilde{G}(t) = \frac{1}{1 - t/1.3}. \quad (16)$$

Now, the dashed lines in Fig. 4 shows the calculations with π , f_2 and soft and hard Pomeron exchanges in comparison with experimental results on differential $\gamma+p \rightarrow \omega+p$ cross section as a function of four momentum transfer squared. The full model results well reproduce the data. The dashed lines in Fig. 5 also show the full model calculations for the forward and total ω -meson

photoproduction. Agreement between the experimental results and the Regge theory calculation is excellent at E_γ from $\simeq 5$ GeV and up to DESY ZEUS energies. Moreover, the contribution from π -meson exchange strongly decreases with energy.

Next we investigate down to which photon energy Regge theory can reproduce available data on differential cross section for ω -meson photoproduction.

Fig. 6 shows the calculations together with the experimental results [23, 26] collected at photon energies from 2.8 to 4.8 GeV. The contribution from Pomeron exchange is indicated by the solid lines, the sum of f_2 and Pomeron exchanges is shown by the dotted lines. The dashed lines in Fig. 6 show the full model results with inclusion of π , f_2 and Pomeron exchanges and well describe the data even at very low photon energies. It is expected that π -meson exchange becomes dominant with decreasing E_γ and at small $|t|$.

Fig.7 shows data [23, 28] on differential $\gamma+p \rightarrow \omega+p$ cross section as a function of four momentum transfer squared collected at different photon energies within the

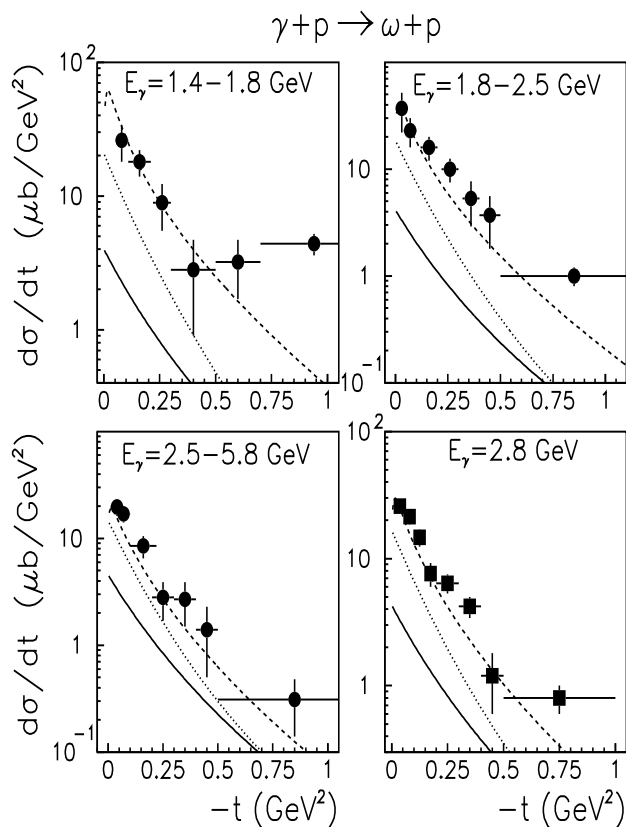


FIG. 7: Differential $\gamma+p \rightarrow \omega+p$ cross section as a function of four momentum transfer squared t at different photon energies E_γ . Squares are the SLAC data [23], while the circles show DESY experimental results [28]. The solid lines indicate the calculations with Pomeron exchange, the dotted lines show the results with additional inclusion of f_2 -meson exchange, while the dashed line are the full model results with π , f_2 and Pomeron exchanges.

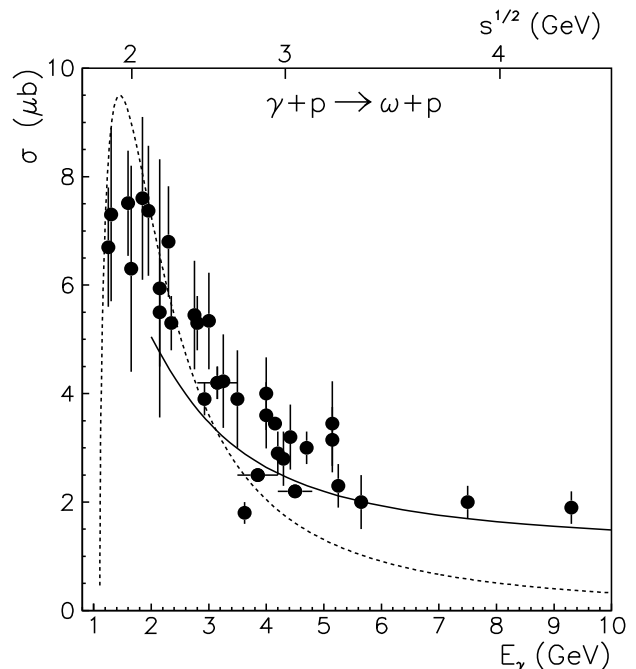


FIG. 8: Total $\gamma+p \rightarrow \omega+p$ cross section as a function of photon energy E_γ . The solid lines indicate the calculations with Regge theory, while the dashed line show meson exchange model results [29].

range $1.4 \leq E_\gamma \leq 5.8$ GeV. The contribution from Pomeron exchange is shown by the solid lines and it is almost negligible. The sum of π , f_2 and Pomeron exchanges are shown by the dashed lines and can describe well the data. Again, the ω -meson photoproduction here is dominated by the π -meson exchange.

IV. CONCLUSION

Analysis of the ω -meson photoproduction data and comparison to Regge theory calculations show that at photon energies above 20 GeV the reaction is entirely dominated by Pomeron exchange. However, we found that Pomeron exchange model can not reproduce the $\gamma+p \rightarrow \rho+p$ and $\gamma+p \rightarrow \omega+p$ data simultaneously with the same set of parameters.

At $E_\gamma < 5$ GeV the dominant contribution to $\gamma+p \rightarrow \omega+p$ reaction comes from π and f_2 -meson exchanges. It is clear that appropriate parameterization of the form factors and coupling constants at the interaction vertices allows us to reproduce the data even at very low energies. Instead of parameterization of the π and f_2 -meson exchanges amplitudes it is possible to describe the ω -meson photoproduction at $E_\gamma < 5$ GeV by meson exchange model [29].

Fig. 8 shows the data on total $\gamma+p \rightarrow \omega+p$ cross section at low photon energies together with the Regge theory calculations and meson exchange model results [29].

Apparently there is smooth transition between the meson exchange model at low energies and Regge theory at high energies.

Finally at $E_\gamma < 5$ GeV and for small momentum transfers the ω -meson photoproduction can be well described by both Regge theory and by meson exchange model.

-
- [1] A. Donnachie and P.V. Landshoff, Phys. Lett. B **348**, 213 (1995).
 - [2] A. Donnachie and P.V. Landshoff, Phys. Lett. B **478**, 146 (2000).
 - [3] J.M. Laget, Phys. Lett. B **489**, 313 (2000).
 - [4] J. Breitweg et al., Eur. Phys. J. C **1**, 81 (1998).
 - [5] A. Donnachie and P.V. Landshoff, Phys. Lett. B **470**, 243 (1999).
 - [6] M. Battaglieri et al., Phys. Rev. Lett. **87**, 172002 (2001).
 - [7] E. Anciant et al., Phys. Rev. Lett. **85**, 4682 (2000).
 - [8] J.M. Laget, Nucl. Phys. A **699**, 184 (2002).
 - [9] A. Sibirtsev, Tsushima and A.W. Thomas, Phys. Rev. C **63**, 044906 (2001).
 - [10] A.C. Irving and R.P. Worden, Phys. Rep. **34**, 117 (1977).
 - [11] M.A. Pichowsky and T.S.H. Lee, Phys. Rev. D **56**, 1644 (1997).
 - [12] A. Donnachie and P.V. Landshoff, Nucl. Phys. B **311**, 509 (1988).
 - [13] A. Donnachie and P.V. Landshoff, Nucl. Phys. B **244**, 322 (1984).
 - [14] A. Donnachie and P.V. Landshoff, Nucl. Phys. B **267**, 690 (1986).
 - [15] J.M. Laget and R. Mendez-Galain, Nucl. Phys. A **581**, 397 (1995).
 - [16] A. Donnachie and P.V. Landshoff, Phys. Lett. B **296**, 227 (1992).
 - [17] G. Veneziano, Nuov. Cim. **57A**, 190 (1968).
 - [18] A.M. Breakstone, Phys. Rev. Lett. **47**, 1782 (1981).
 - [19] M. Derrick et al., Z. Phys. C **73**, 73 (1996).
 - [20] A. Sibirtsev, S. Krewald and K. Tsushima, Proc. Meson 2002 7 Int. Workshop on Production, Properties and Interactions of Meson, Cracow, nucl-th/0208015.
 - [21] A. Donnachie and P.V. Landshoff, Phys. Lett. B **348**, 213 (1995).
 - [22] A. Sibirtsev and W. Cassing, Eur. Phys. J. A **7**, 407 (2000).
 - [23] J. Ballam et al., Phys. Rev. D **7**, 3150 (1973).
 - [24] J. Abramson et al., Phys. Rev. Lett. **36**, 1428 (1976).
 - [25] J. Busenitz et al, Phys. Rev. D **40**, 1 (1989).
 - [26] D.P. Barber et al., Z. Phys. C **26**, 343 (1984).
 - [27] A.C. Irving and C. Michael, Nucl. Phys. B **82**, 282 (1974).
 - [28] R. Erbe et al., Phys. Rev. **175**, 1669 (1968).
 - [29] A. Sibirtsev, K. Tsushima and S. Krewald, nucl-th/0202083.